Available online at www.sciencedirect.com

ScienceDirect

www.elsevier.com/locate/jes

JES JOURNAL OF ENVIRONMENTAL SCIENCES

www.jesc.ac.cn

# Newly developed $Fe_3O_4$–$Cr_2O_3$ magnetic nanocomposite for photocatalytic decomposition of 4-chlorophenol in water

*Khoirakpam Kesho Singh*[1], *Kula Kamal Senapati*[2,3,*], *Chandan Borgohain*[1], *Kanak Chandra Sarma*[1]

1. *Department of Instrumentation and USIC, Gauhati University, Guwahati 781014, Assam, India. E-mail: kesho.singh81@gmail.com*
2. *Central Instruments Facility, Indian Institute of Technology Guwahati, Guwahati 781039, Assam, India*
3. *Department of Biochemistry, Tocklai Tea Research Institute, TRA, Jorhat 785008, Assam, India*

ARTICLE INFO

*Article history:*
Received 10 October 2014
Revised 28 December 2014
Accepted 14 January 2015
Available online 29 August 2015

*Keywords:*
Chlorophenol
Magnetic nanocomposite
Photocatalyst
Core/shell nanocomposite

ABSTRACT

Chlorophenols, typically 4-chlorophenols are highly toxic and non-biodegradable organic contaminants which pose serious threat to the environment, particularly when released into aqueous medium. The removal of these pollutants by efficient method has received worldwide concern in recent past. A new $Fe_3O_4$–$Cr_2O_3$ magnetic nanocomposite was synthesized by wet chemical method under ultrasonic irradiation. Microstructure and morphology of the nanocomposite were characterized by powder X-ray diffraction (XRD), Fourier transform infrared (FT-IR), and a transmission electron microscope (TEM). Magnetic and optical properties were studied by a vibrating sample magnetometer (VSM) and an ultraviolet–visible (UV–Vis) spectrophotometer respectively. The magnetic nanocomposite (MNC) was used as photocatalyst for effective decomposition of 4-chlorophenol in water under ultraviolet (UV) irradiation.



## Introduction

Magnetic nanocomposites (MNCs) are hybrid structures with improved chemical and physical properties and have been extensively used in numerous catalytic reactions besides their popular use in many technological fields such as magneto-optical device, solar cells, biomedical engineering, chemical sensing *etc.* (Zhu et al., 2010). These nanomaterials offer significant advantage in catalysis of being separated by external magnetic field, thereby eliminating the catalyst filtration after completion of the reaction and thus easy recycling making it cost-effective for the catalytic reaction. Out of the MNCs, core/shell structured materials have attained considerable interest in heterogeneous catalysis *e.g.* photochemical degradation of organic contaminants in waste water (Tian et al., 2011; Senapati et al., 2012). In these materials, the shell component plays the role of an active catalyst and the magnetic core component imparts easy recovery of the whole composite material by an external magnet along with its crucial role in electron-hole ($e^-/h^+$) pair mechanism in photocatalysis (Chen et al., 2008).

It is known that chromium(III) oxide ($Cr_2O_3$) is a p-type semiconductor with wide band gap energy (~3 eV) and shows high electrical conductivity as well as high thermal and chemical stability (Santulli et al., 2011). It is used in industry as a refractory, high-temperature oxidation resistance material (Cao et al., 2006) and as catalysts (Cherian et al., 2002; Hammoudeh et al., 2006). On the other hand, magnetite ($Fe_3O_4$) is an n-type semiconducting oxide with narrow band gap energy (ca. 0.14 eV) (Cabot et al., 2007). It is a biocompatible (non-toxic) and environmental friendly oxide and in addition to the catalytic applications, it is widely used in biotechnology-biomedicine

* *Corresponding author*. E-mails: kulakamal@yahoo.co.in, kulasenapati@gmail.com (Kula Kamal Senapati).

http://dx.doi.org/10.1016/j.jes.2015.01.035

including magnetic fluid hyperthermia, targeted drug delivery, magnetic resonance imaging and so on (Zhang and Du, 2006; Ma and Liu, 2007; Gupta and Gupta, 2005). So, designing and fabricating the hybrid magnetic nanomaterial of antiferromagnetic $Cr_2O_3$ and ferromagnetic $Fe_3O_4$ core/shell structure will impart a highly functional material. The magnetic core material of the nanocomposite can act as an anchor to separate the composite material magnetically and thus lead to easily recyclable catalyst in addition to its role in photoactivity with $Cr_2O_3$ shell. In recent past, synthesis of magnetic nanocomposite of $Fe_3O_4$ and $Cr_2O_3$ were reported where mechanical alloying (Liu et al., 2008) and combined mechanical and sonochemical (Yun et al., 2009) routes were employed. Although nanocomposite of core/shell type structure with $Cr_2O_3$ core and $Fe_3O_4$ shell was synthesized, the magnetic nanocomposite of $Fe_3O_4$ core and $Cr_2O_3$ shell structure has not been addressed so far. Herein, we report the synthesis of $Fe_3O_4$–$Cr_2O_3$ core/shell structure following a similar protocol to the synthesis of $CoFe_2O_4$–$Cr_2O_3$ core/shell nanocomposites as reported earlier (Senapati et al., 2011; Borgohain et al., 2010).

Now it is more widely accepted that the phenols and substituted phenols are one of the most highly toxic water contaminant and to control the environmental pollution by these pollutants is a major challenge in today's technology. The chlorophenols (CPs) are mostly used in pesticides, fungicides, herbicides, dyes, and solvents and are hardly biodegradable, and difficult to remove from the environment (Ramamoorthy and Ramamoorthy, 1997). Moreover, 4-chlorophenol (4-CP) is the precursor of many highly toxic organic compounds (Theurich et al., 1996). Because of their many origins, CPs can be found in ground water, wastewater, and soil and thus their contamination is highly concerned. In past two decades, photocatalysis by metal oxide/chalcogenide semiconductors, such as $TiO_2$, ZnO, $Cu_2O$, CuS *etc.*, have been widely employed in degradation of various organic pollutants from aqueous medium (Cheng et al., 2007; Jing et al., 2001; Tang et al., 2008; Li et al., 2010). Photocatalytic degradation of phenolic compounds has gained priority over other catalytic processes as photocatalysis proves to perform complete mineralization of organic compounds. Therefore, the newly developed magnetic nanocomposite opens an avenue to eliminate the chlorinated phenols from the contaminated water in an easy and cost-effective process.

In the present work, we report the synthesis of $Fe_3O_4$–$Cr_2O_3$ core/shell nanocomposite by an ultrasound assisted wet chemical method. Further, we investigate the efficiency of the magnetic composites as photocatalyst in degradation of 4-CP in aqueous medium under ultraviolet (UV) irradiation.

## 1. Experimental Section

### 1.1. Materials

$FeCl_2 \cdot 4H_2O$ (extra pure, AR grade, LobaChemie), $FeCl_3 \cdot 6H_2O$ (99%, LobaChemie), NaOH (99%, Merck India), $Cr_3(OH)_2(CH_3COOH)_7$ (Cr 24%, Alfa Aesar), Ethyl alcohol (99.5%, Tedia), and 4-chlorophenol (99%, Sigma) were used directly without further purification.

## 2. Methods

Synthesis of $Fe_3O_4$–$Cr_2O_3$ core/shell nanocomposite involved two steps: in the first step, $Fe_3O_4$ MNPs were synthesized by co-precipitation method (Massart, 1981) under ultrasonic irradiation, and in the second step coating of a thin layer of $Cr_2O_3$ was deposited on the surface of $Fe_3O_4$ MNPs. The detailed procedure is as follows.

A mixture of 2.7 g of $FeCl_3 \cdot 6H_2O$ and 1.0 g of $FeCl_2 \cdot 4H_2O$ (molar ratio of $Fe^{2+}$:$Fe^{3+}$ = 1:2) was dissolved in 50 mL of deoxygenated deionized water in a 100 mL flat bottom flask under nitrogen atmosphere and the solution was kept under ultrasonic irradiation at frequency 20 kHz and power 40 kW. An aqueous solution of 1 mol/L NaOH was added drop-wise continuously until a thick black precipitate formed and the sonication was continued for another 30 min to obtain stable colloidal particles. The as formed $Fe_3O_4$ particles were separated by centrifugation at 10,000 r/min and washed several times with de-ionized water till to obtain neutral pH of the filtrate and finally washed with dried ethanol. The particles were dried in a vacuum oven at 100°C for 24 hr and then kept in a desiccator for further analysis.

In the second step, 0.075 g of $Fe_3O_4$ NPs was dispersed ultrasonically in the 50 mL aqueous solution containing 0.066 g $Cr_3(OH)_2(CH_3COO)_7$. An aqueous solution of 1 mol/L NaOH was added drop-wise continuously into the above solution mixture under ultrasonic irradiation until dark green gelatinous precipitates formed. Precipitate was washed several times with de-ionized water, finally with dried ethanol and dried in vacuum oven at 100°C for overnight. The dried sample was then annealed at 500°C for 5 hr under constant nitrogen gas flow so as to obtain crystalline $Fe_3O_4$–$Cr_2O_3$ nanocomposite. The same procedure was followed in incorporation of different mass ratios of $Cr_2O_3$ to $Fe_3O_4$ by mixing 0.075 g of as-prepared $Fe_3O_4$ nanoparticles with the 0.066, 0.019, 0.079, and 0.097 g of $Cr_3(OH)_2(CH_3COO)_7$ respectively.

### 2.1. Characterization

X-ray diffraction (XRD) patterns of the nanocomposite was recorded using a powder X-ray diffractometer (X'Pert Pro, Philips, USA) with Cu $K\alpha$ as radiation source, where, $\lambda$ = 0.154 nm, scan range ($2\theta$): 20–70° with a scan step size of 0.04. The infrared (IR) analysis was carried out by a Fourier transform infrared (FT-IR) (RXI, Perkin Elmer, USA) spectrometer using KBr pellet. The morphology and size were analyzed by a transmission electron microscope (TEM) (JEM-2100, JEOL, Japan) operating at 200 kV. Room temperature magnetic property measurement was carried out by vibrating sample magnetometer (VSM, 7410, Lakeshore, USA). The spectrophotometric measurements were performed on a UV–Vis spectrophotometer (Cary 50, Varian, USA). The specific surface area of the magnetic nanocomposite was determined by a BET surface area analyser (ChemiSorb 2720, Micromeritics, USA). Prior to surface area analysis, 0.025 mg of the sample was dried at 100°C under helium atmosphere for 1 hr. The mass (or weight) ratio and stoichiometry of the as-prepared $Fe_3O_4$–$Cr_2O_3$ core/shell nanocomposites were investigated by energy dispersive X–ray spectroscopy (EDX) (Leo 1430vp, Oxford Instruments, UK).

### 2.2. Photocatalytic Activity Measurement

The photocatalytic activity of the $Fe_3O_4$–$Cr_2O_3$ nanocomposites were evaluated by degradation of aqueous solution of 4-CP under UV irradiation (12 W, low pressure mercury lamp). Prior to UV-irradiation, the $Fe_3O_4$–$Cr_2O_3$ MNC (2 g/L) was dispersed in 50 mL aqueous solution of 4-CP ($10^{-2}$ mmol/L) in a reaction vessel and stirred continuously in the dark for 30 min in order to attain an adsorption/desorption equilibrium. Then the solution was placed in a UV lamp chamber under UV-irradiation while the solution was constantly stirring. The ambient temperature was maintained by an outer jacket of water circulation though the solution. During photocatalysis, an aliquot of 4-CP solution was extracted in every 30 min and separated the suspended catalyst magnetically by using an external magnet to take the absorbance measurement in a UV–Vis spectrophotometer. The degradation efficiency of 4-CP ($R$) was calculated from the following expression (Wang et al., 2004):

$$R = \frac{A_O - A}{A_O} \times 100\%$$

where, $A_O$ represents the initial absorbance of the solution, and $A$ is the absorbance of the solution after irradiation time ($t$).

### 2.3. Degradation Analysis by Liquid Chromatography Mass Spectrometry (LCMS)

The LCMS analysis (QTOF LCMSMS LCMS, Waters, USA) was carried out with a binary pump, T-UV–Vis diode array detector, an autosampler, and a column thermostat. The LCMS system was equipped with a C18 column (Acquity UPLC™ BEH C18 1.7 μm, 2.1 mm × 50 mm column). The gradient HPLC separation was coupled with Electrospray ionization (ESI)-mass. The solvent used as mobile phase was acetonitrile:water (1:1). The solvent flow rate was set at 0.3 mL/min with 30 μL of injection volume of the standard or sample solution through the column. High purity nitrogen (99.99%) and argon (99.999%) were used as a nebulizer (API gas) and collision cell gas respectively. Mass spectrometry was used to detect the parent ion and/or molecular ions and fragmented ions formed during photo-degradation of 4-CP. Prior to analysis, 2 mL aliquots of initial 4-CP aqueous solution and the solution after degradation (separated from the catalyst by magnetic decantation) were filtered through a 0.2 μm pore size polypropylene membrane filter. Before starting the sample analysis, an instrument was calibrated with sodium formate standard solution (Fluka) in the mass range, 100–1000 $m/z$ for both ESI positive and negative ion mode. Following tuning parameters of the instrument were set for the mass analysis: Capillary (kV), 2.5; sampling cone, 15; source temperature (°C), 120; dissolvation temperature (°C), 150; collision energy, 5.0; ionization mode, ESI; optics, V mode and the others remaining parameters were left to default settings.

## 3. Results and Discussion

### 3.1. Characterization of $Fe_3O_4$–$Cr_2O_3$ MNCs

To investigate the microstructure and morphology of the core/shell nanocomposite, following spectroscopic and non-spectroscopic analyses were carried out. Fig. 1 shows the X-ray diffraction pattern of $Fe_3O_4$–$Cr_2O_3$ nanocomposite. It can be seen from the figure that diffraction peaks and relative intensities of the pattern match well with the cubic inverse spinel structure of $Fe_3O_4$ (International center for diffraction data, JCPDS-PDF Card No. 65-3107) and that of $Cr_2O_3$ (ICDD, JCPDS PDF Card No. 74-0326) nanoparticles.

Fig. 2 represents the IR spectrum of (a) $Fe_3O_4$ nanoparticles and (b) $Cr_2O_3$–$Fe_3O_4$ MNCs. The peaks at 569 and 3415 $cm^{-1}$ are related to the characteristic absorption of Fe–O bond in $Fe_3O_4$ (Kim et al., 2009) and the stretching vibration of surface bound OH group (Hoa et al., 2009) respectively. IR bands at 631 and 578 $cm^{-1}$ are associated with Cr–O vibration in α-$Cr_2O_3$ (Znaidi and Pommier, 1998). Peak observed at 1627 $cm^{-1}$ in both spectra is related to the characteristics δOH vibration in water molecules (Tie et al., 2007).

Transmission electron micrograph of $Fe_3O_4$–$Cr_2O_3$ core/shell nanocomposite is shown in Fig. 3a. It is observed that MNCs are nearly regular in shape with average particles size of 50 ± 5 nm. It is also seen from the image that a very thin and contrast layer appeared on the outer surface of nanoparticles indicates the $Cr_2O_3$ shell. The selected area electron diffraction (SAED) pattern of the MNC is shown in the Fig. 3b. The rings corresponding to the lattice planes (220) and (440) can be indexed as cubic phase of $Fe_3O_4$ NPs. Similarly, the rings (012), (024), and (300) can be indexed with α-$Cr_2O_3$. The elemental weight composition of O, Cr, and Fe in the $Fe_3O_4$–$Cr_2O_3$ nanocomposites as determined by EDX analysis (Fig. S4) was found to be 30.17%, 10.13%, and 59.70% respectively and the mass ratio of $Fe_3O_4$ to $Cr_2O_3$ was found to be nearly 1:0.3. The oxygen content in the EDX analysis was found to be slightly higher than expected theoretically which might be due to adsorbed oxygen in the nanocomposite surface. The BET specific surface area the $Fe_3O_4$–$Cr_2O_3$ MNCs was determined to be 36.9905 $m^2/g$.

### 3.2. Magnetic Property Measurement

The magnetic hysteresis (MH) loops of the $Fe_3O_4$ and $Fe_3O_4$–$Cr_2O_3$ samples were recorded at room temperature with maximum applied field of ±2 T (as shown in Fig. 4). From the hysteresis loop, the saturation magnetization ($M_s$), coercivity ($H_c$), and retentivity ($M_r$) values were determined. A saturation magnetization of 66.26 emu/g for $Fe_3O_4$ nanoparticles was observed which is less than the reported value of the bulk $Fe_3O_4$ particles (92 emu/g) (Tie et al., 2007). It is known that,

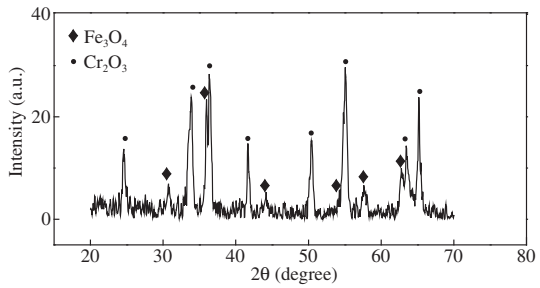


**Fig. 1 – X-ray diffraction pattern of $Fe_3O_4$–$Cr_2O_3$ core/shell magnetic nanocomposite (MNC).**

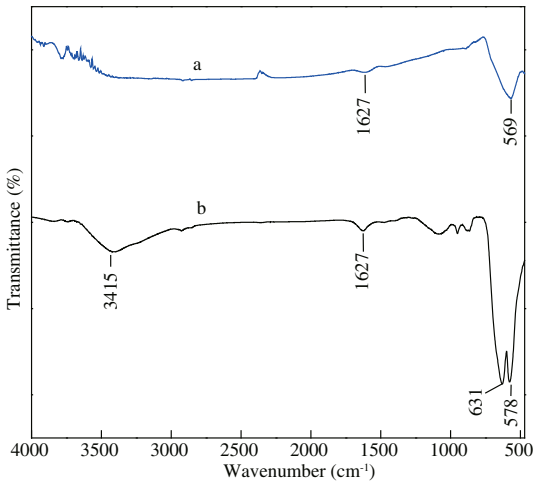


**Fig. 2 – Infrared spectrums of (a) $Fe_3O_4$ nanoparticles (NPs) and (b) $Fe_3O_4$–$Cr_2O_3$ MNC. MNC: magnetic nanocomposite.**

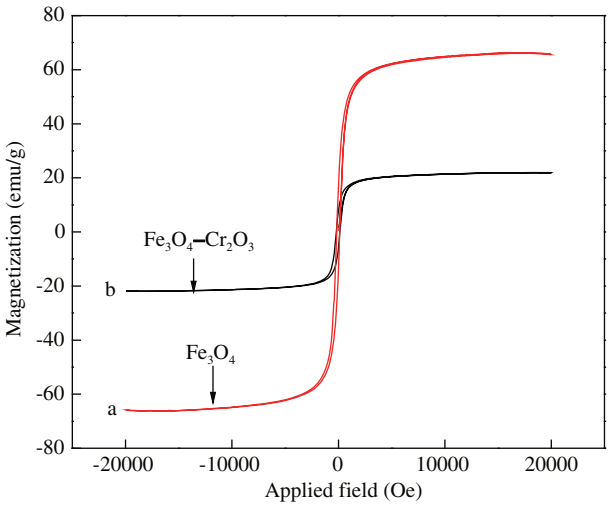


**Fig. 4 – Room temperature magnetic hysteresis (MH) loops of (a) $Fe_3O_4$ and (b) $Fe_3O_4$–$Cr_2O_3$.**

magnetite ($Fe_3O_4$) is a ferrimagnet having cubic inverse spinel structure with tetrahedral sites are occupied by $Fe^{3+}$ ions and the octahedral sites are occupied by the even mix of $Fe^{3+}$ and $Fe^{2+}$ ions. This inverse spinel structure may be represented by the formula $(Fe^{3+})_{tet}[Fe^{2+}, Fe^{3+}]_{oct}O_4$ (Tirosh et al., 2006). The magnetic contributions of the tetrahedral and octahedral $Fe^{3+}$ cations are mutually compensated so the net magnetism in $Fe_3O_4$ is solely dependent on the magnetic moment contributed by octahedral $Fe^{2+}$ ions of the unit cell (Garcia and Subias, 2004). Herein, ferromagnetic behavior has been observed in case of $Fe_3O_4$–$Cr_2O_3$ at room temperature. It can be seen from Table 1 that, incorporation of $Cr_2O_3$ into the Fe–O matrix has very little effect on coercivity, however saturation magnetization and retentivity decrease sharply. Therefore, by controlling the thickness of $Cr_2O_3$ shell, the magnetic properties of the $Fe_3O_4$–$Cr_2O_3$ may be tuned to suit various applications.

### 3.3. UV–Vis Analysis

UV–Vis spectra of as prepared $Fe_3O_4$–$Cr_2O_3$ and $Cr_2O_3$ samples in aqueous dispersions are shown in Fig. 5. For each sample two distinct absorption bands appeared around 270 and 370 nm in the spectrum. Since $Cr_2O_3$ is a semiconductor, and its highest occupied molecular orbital (HOMO) is termed as valence band (VB) and the lowest unoccupied molecular orbital (LUMO) is termed as conduction band (CB), we believe that absorption band at 270 nm corresponds to charge transfer between the HOMO of O2p and the LUMO of Cr3d, while absorption peak at 370 nm is originated from d–d transition in $Cr^{3+}$ ($3d^3$) of $Cr_2O_3$ (Kim et al., 2000).

The optical band-gap of newly synthesized nanocomposite was evaluated from the manipulation of the UV–Vis absorption spectra using following equation for direct transitions (Hameed et al., 2009): $(\alpha h\nu) = \text{const}(h\nu - E_g)^{\frac{1}{2}}$ where "$h\nu$" is the photon energy and the "$E_g$" is the band-gap energy. The absorption co-efficient "α" was evaluated according to the equation:

$$\alpha = 2.3026 \times \frac{A}{t}$$

where "t" is the optical path length and "A" is the absorbance.

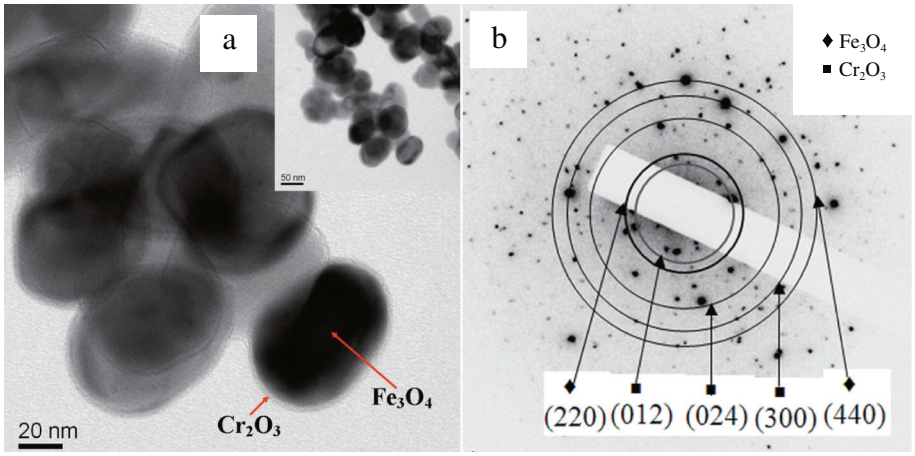


**Fig. 3 – Transmission electron micrograph of (a) $Fe_3O_4$–$Cr_2O_3$ core/shell nanocomposite and (b) corresponding selected area electron diffraction (SAED) pattern.**

**Table 1 – Effect of incorporation of antiferromagnetic $Cr_2O_3$ into the Fe–O matrix on its magnetic properties.**

| Sample | $M_s$ (emu/g) | $H_c$ (Oersted) | $M_r$ (emu/g) |
|---|---|---|---|
| $Fe_3O_4$ | 66.26 | 163.04 | 16.79 |
| $Fe_3O_4$–$Cr_2O_3$ | 21.94 | 171.94 | 6.84 |

$M_s$: saturation magnetization; $H_c$: coercivity; $M_r$: retentivity.

The plot of $(\alpha h\nu)^2$ *versus* photon energy ($h\nu$) for each $Fe_3O_4$–$Cr_2O_3$ nanocomposite and pure $Cr_2O_3$ is shown in Fig. 5 (inset). The band-gap energy was evaluated by extrapolating the linear portion of the curve to $(\alpha h\nu)^2 = 0$. The estimated value of band-gap energy for $Fe_3O_4$–$Cr_2O_3$ nanocomposite is 2.94 eV, which is slightly less than the value for pure $Cr_2O_3$ (3.05 eV). This shifting of band-gap energy to lower energy range was due to the effect of hetero-junction formed at the interface between $Fe_3O_4$ (n-type semiconductor) and $Cr_2O_3$ (p-type semiconductor) in $Fe_3O_4$–$Cr_2O_3$ nanocomposite (Borgohain et al., 2012).

### 3.4. Photocatalytic Activity Measurement

We studied the degradation of 4-CP by $Fe_3O_4$–$Cr_2O_3$ MNCs under UV irradiation. The $Fe_3O_4$–$Cr_2O_3$ nanoparticles with composition ratio $Fe_3O_4$:$Cr_2O_3$ = 1:0.3 exhibited the highest photocatalytic efficiency in photodegradation of 4-chlorophenol in water. The degradation profile of the 4-CP at different time intervals of UV irradiation is presented in Fig. 6.

It was noticed that the degradation of the 4-CP by the $Fe_3O_4$–$Cr_2O_3$ MNC was approximately 20% in the first 0.5 hr, 50% in 1.5 hr, and finally nearly 100% in 2.5 hr of UV irradiation. From the UV–Vis absorption spectra (Fig. 6), it is seen that no absorption bands appeared in the UV region after complete degradation of the compound, indicating the break-down of the aromatic ring of 4-CP and thereafter complete mineralization took place. The catalyst was separated easily from the aqueous medium by the use of an external magnet (Fig. S1), and then was

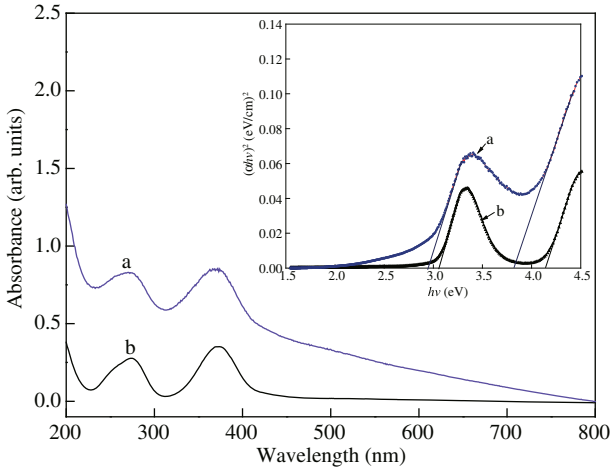


**Fig. 5 – UV–Vis absorbance spectra (a) $Fe_3O_4$–$Cr_2O_3$ and (b) $Cr_2O_3$. Inset shows the corresponding plot of $(\alpha h\nu)^2$ *versus* photon energy ($h\nu$). UV–Vis: ultraviolet–visible.**

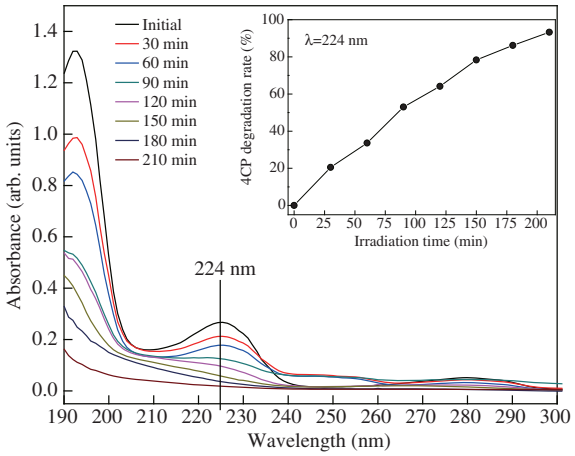


**Fig. 6 – Degradation profile of 4-chlorophenol (4-CP) in the presence of $Fe_3O_4$–$Cr_2O_3$ MNC under UV irradiation. MNC: magnetic nanocomposite; UV: ultraviolet.**

washed several times with dried ethanol and dried for further use. The reusability of the catalyst was checked up to four catalytic cycles and no loss of catalytic activity was observed (Fig. S2).

The high photocatalytic activity of $Fe_3O_4$–$Cr_2O_3$ nanocomposite is due to high band-gap energy (2.94 eV) and the formation of hetero-junction (p–n junction) between the $Fe_3O_4$ and $Cr_2O_3$ interface. Earlier, Chen et al. (2008) demonstrated the formation of hetero-junction in the interface between p-type and n-type semiconductors which can suppress the recombination of photo-generated $e^-/h^+$ pairs and thus enhance the photocatalytic efficiency. It is known that $Cr_2O_3$ is a p-type semiconductor (Santulli et al., 2011) while magnetite ($Fe_3O_4$) is an n-type semiconductor (Cabot et al., 2007). Since the band-gap energy of $Fe_3O_4$ is lower with slightly smaller work function (5.78 eV) (Fonin et al., 2005) in comparison to the work function of $Cr_2O_3$ (5.9 eV) (Krylov, 1970), the Fermi level of $Cr_2O_3$ is lower than that of $Fe_3O_4$. The band edges of $Fe_3O_4$ and $Cr_2O_3$ at the interface shift to adjust the Fermi level until equilibrium is attained. A positive shift in the Fermi level of $Fe_3O_4$ and a negative shift in the Fermi level of $Cr_2O_3$ are expected. An inner field is created at the interface which causes the electrons to move from $Cr_2O_3$ to $Fe_3O_4$ leaving the $Cr_2O_3$ region with positive charges and the $Fe_3O_4$ region with negative charges. Based on this argument, an energy band structure diagram of the $Fe_3O_4$–$Cr_2O_3$ heterojunction is shown schematically in Fig. 7.

When the $Fe_3O_4$–$Cr_2O_3$ heterojunction was excited by UV light with photon energy ($h\nu$) higher or equal to the band gaps of $Cr_2O_3$ and $Fe_3O_4$, the electrons in the valence band (VB) moved to the conduction band (CB) generating equal amount of holes in VB. This process transfers the photogenerated electrons from the CB of $Fe_3O_4$ to the CB of $Cr_2O_3$. On the contrary, the photogenerated holes transfer takes place from the VB of $Cr_2O_3$ to the VB of $Fe_3O_4$. This suggests that the photogenerated electrons and holes in the heterojunction were efficiently separated. The excess valance band electrons then migrate to the surface of $Cr_2O_3$ and react with the

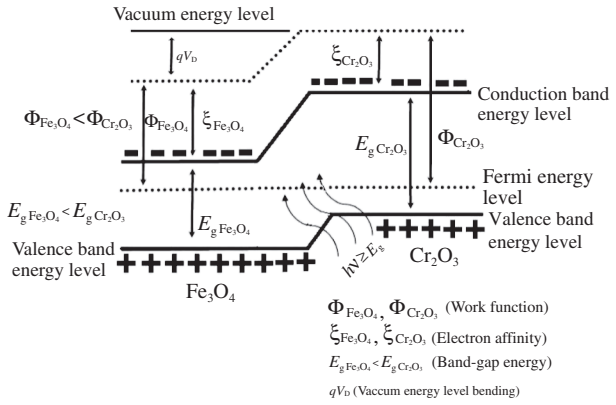


**Fig. 7 – Schematic illustration of the energy level and band-gap structure of $Fe_3O_4$–$Cr_2O_3$, when the $Fe_3O_4$–$Cr_2O_3$ heterojunction was excited by UV light with photon energy ($h\nu$). UV: ultraviolet.**

trapped $O_2$ to produce superoxide radical anions, $O^{2-}$, which on protonation generates hydroxyl radical, $OH^{\cdot}$. Similarly, the holes that were transferred to the $Fe_3O_4$ react with the trapped by surface hydroxyl groups (or $H_2O$) in $Fe_3O_4$ to yield $OH^{\cdot}$ radicals (Borgohain et al., 2012). These $OH^{\cdot}$ radicals are highly reactive to degrade organic molecular in water and can enhance the photocatalytic activity of the material.

### 3.5. *LCMS Analysis*

The degradation of 4-CP was further studied by the liquid chromatography coupled with mass spectrometry. The chromatographic separation was recorded for the 4-CP solution initially and after 2.5 hr of photocatalytic treatment at 224 nm wavelength using diode array detector (TUV) (Fig. S3(a–b), extracted UV peaks in inset). The 4-CP solution gave two significant peaks at retention times (r.t.) of 0.60 min and 5.51 min corresponding to the solvent and 4-CP molecule (with the extracted UV peak in the inset). However, we didn't observe any peak of significant intensity at r.t. of 5.51 min for the 4-CP molecule after the photocatalysis except the peak at r.t. 0.75 min (Fig. S3b) which was due to the solvent present in 4-CP solution before and after the degradation. Moreover, the LC-UV chromatogram (inset of Fig. S3b) showed no absorption peak of 4-CP and only the maximum absorption was detected at the wavelength of 214 nm which was attributed from the solvent and its contamination. This experimental data implied that after UV irradiation of 2.5 hr in the presence of the photocatalyst, the 4-CP was significantly degraded. Thus, the liquid chromatography coupled with UV absorbance using a diode array detector clearly showed that, the 4-CP was appreciably degraded into small molecules such as $CO_2$, HCl, $H_2O$ *etc.* which could not be detected by LCMS analysis.

To understand the intermediate products formed during photo-degradation of the 4-CP, we extracted aliquot amount of sample after 1 hr of UV irradiation and performed the ESI-mass analysis, and the data were presented in Fig. 8b. The positive ion mode signals at 110 and 117 *m/z* belonged to hydroquinone (HQ) and hydroxyl-hydroquinone (HHQ) respectively. The plausible photocatalytic degradation of 4-CP described in our manuscript is based on the degradation pathway as described by Li et al. (1999). Photocatalytic degradation is an oxidative process, and given the facile oxidation of hydroquinone to benzoquinone under ordinary conditions. The formation and destruction of two major intermediates *i.e.* HQ and benzoquinone (BQ) was also reported by Bahnemann et al. (Theurich et al., 1996). The other major compounds detected in this case were: 1, 2, 4-benzenetriol (*m/z* 126), α-ketosuccinic acid (*m/z* 131) *etc.*, and their fragmented aliphatic products which are in good agreement with the results of other research groups (Theurich et al., 1996; Li et al., 1999). The parent molecular ion peak of 4-CP at 127 *m/z* as detected before the UV-irradiation of the 4-CP solution as shown in Fig. 8a was not observed after the irradiation.

Based on the above observations, the probable photocatalytic degradation of 4-CP similar to the pathway described by Li et al. (1999) is depicted in Scheme 1. During photocatalytic process, the photogenerated holes ($h^+_{BV}$) on the catalyst surface under UV irradiation are scavenged by surface adsorbed hydroxyl group ($OH^-$) to generate highly oxidative hydroxyl radical ($HO^{\cdot}$). These hydroxyl radicals and solvated hydroxyl radicals are the main oxidant to react with 4-CP and

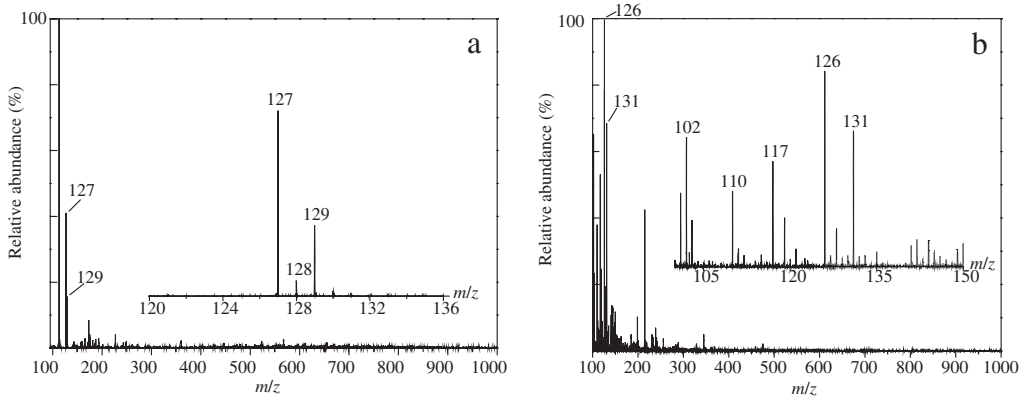


**Fig. 8 – Electrospray ionization (ESI) mass spectra of 4-chlorophenol (4-CP) at initial (0 hr) (a) and after 1 hr (b) of UV irradiation. UV: ultraviolet.**

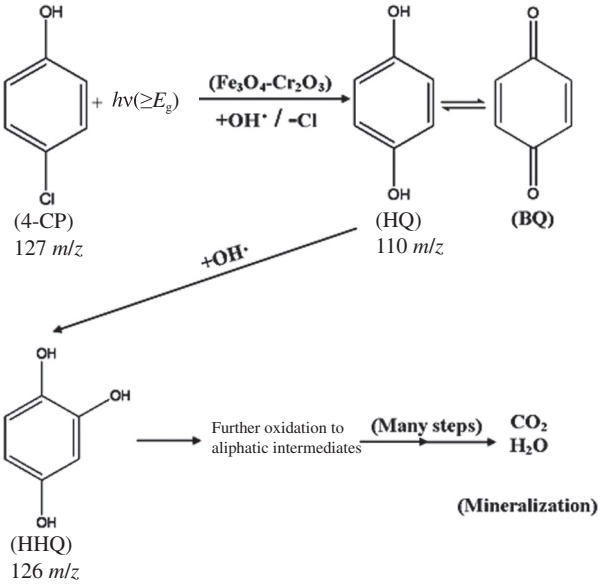


**Scheme 1 – Plausible degradation pathways of photodegradation of 4-chlorophenol (4-CP) in the presence of $Fe_3O_4$–$Cr_2O_3$ nanocomposite (Theurich et al., 1996; Li et al., 1999). HQ: hydroquinone; BQ: benzoquinone; HHQ: hydroxyl-hydroquinone.**

convert it first to HQ, then to HHQ and finally complete cleavage of the aromatic ring into smaller molecules such as $CO_2$ and $H_2O$.

## 4. Conclusions

The synthesis of core/shell type $Fe_3O_4$–$Cr_2O_3$ MNC with an average size of 50 ± 5 nm using ultrasonication assisted co-precipitation method was reported. The as-synthesized nanocomposite exhibits efficient photocatalytic activity in degradation of 4-chlorophenol in aqueous solution under UV irradiation. The catalyst is easily magnetically separable, environmentally friendly, sustainable and efficiently reusable alternative catalyst.

## Acknowledgments

Authors appreciate the SAIF, Department of Instrumentation and USIC, Gauhati University for providing powder XRD facility. The authors would also like to acknowledge the support from Central Instruments Facility and Department of Chemistry of Indian Institute of Technology Guwahati for extending various analytical facilities during the course of investigation.

## Appendix A. Supplementary Data

Supplementary data to this article can be found online at http://dx.doi.org/10.1016/j.jes.2015.01.035.

## REFERENCES

Borgohain, C., Senapati, K.K., Mishra, D., Sarma, K.C., Phukan, P., 2010. A new $CoFe_2O_4$–$Cr_2O_3$–$SiO_2$ fluorescent magnetic nanocomposite. Nanoscale 2 (10), 2250–2256.

Borgohain, C., Senapati, K.K., Sarma, K.C., Phukan, P., 2012. A facile synthesis of nanocrystalline $CoFe_2O_4$ embedded one-dimensional ZnO hetero-structure and its use in photocatalysis. J. Mol. Catal. A Chem. 363–364, 495–500.

Cabot, A., Puntes, V.F., Shevchenko, E., Yin, Y., Balcells, L., Marcus, M.A., et al., 2007. Vacancy coalescence during oxidation of iron nanoparticles. J. Am. Chem. Soc. 129 (34), 10358–10360.

Cao, H.Q., Qiu, X.Q., Liang, Y., Zhao, M.J., Zhu, Q.M., 2006. Sol–gel synthesis and photoluminescence of *p*-type semiconductor $Cr_2O_3$ nanowires. Appl. Phys. Lett. 88 (24), 241112.

Chen, S.F., Zhang, S.J., Liu, W., Zhao, W., 2008. Preparation and activity evaluation of p–n junction photocatalyst $NiO/TiO_2$. J. Hazard. Mater. 155 (1-2), 320–326.

Cheng, Y.P., Sun, H.Q., Jin, W.Q., Xu, N.P., 2007. Photocatalytic degradation of 4-chlorophenol with combustion synthesized $TiO_2$ under visible light irradiation. Chem. Eng. J. 128 (2-3), 127–133.

Cherian, M., Rao, M.S., Yang, W., Jehng, J.M., Hirt, A.M., Deo, G., 2002. Oxidative dehydrogenation of propane over $Cr_2O_3/Al_2O_3$ and $Cr_2O_3$ catalysts: effects of loading, precursor and surface area. Appl. Catal. A Gen. 233 (1-2), 21–33.

Fonin, M., Pentcheva, R., Dedkov, Y.S., Sperlich, M., Vyalikh, D.V., Scheffler, M., et al., 2005. Surface electronic structure of the $Fe_3O_4$(100): evidence of a half-metal to metal transition. Phys. Rev. B 72 (10), 104436.

Garcia, J., Subias, G., 2004. The Verwey transition—a new perspective. J. Phys. Condens. Matter 16 (7), R145–R178.

Gupta, A.K., Gupta, M., 2005. Synthesis and surface engineering of iron oxide nanoparticles for biomedical applications. Biomaterials 26 (18), 3995–4021.

Hameed, A., Gombac, V., Montini, T., Graziani, M., Fornasiero, P., 2009. Synthesis, characterization and photocatalytic activity of NiO–$Bi_2O_3$ nanocomposites. Chem. Phys. Lett. 472 (4-6), 212–216.

Hammoudeh, A., Mahmoud, S., Humaidi, J., Wahed, H.A., 2006. Catalytic hydrolysis of CFC-12 over $Cr_2O_3$ catalysts. Jordan J. Chem. 1 (2), 129–142.

Hoa, L.T.M., Dung, T.T., Danh, T.M., Duc, N.H., Chien, D.M., 2009. Preparation and characterization of magnetic nanoparticles coated with polyethylene glycol. J. Phys. Conf. Ser. 187 (1), 012048.

Jing, L.Q., Xu, Z.L., Sun, X.J., Shang, J., Cai, W.M., 2001. The surface properties and photocatalytic activities of ZnO ultrafine particles. Appl. Surf. Sci. 180 (3-4), 308–314.

Kim, E., Jiang, Z., No, K., 2000. Measurement and calculation of optical band gap of chromium aluminium oxide films. Jpn. J. Appl. Phys. 39 (8), 4820–4825.

Kim, M.J., Choa, Y.H., Kim, D.H., Kim, K.H., 2009. Magnetic behaviors of surface modified superparamagnetic magnetite nanoparticles. IEEE Trans. Magn. 45 (6), 2446–2449.

Krylov, O.V., 1970. Catalysis by Nonmetals: Rules for Catalyst Selection. Academic Press, New York, USA.

Li, X., Cubbage, J.W., Tetzlaff, T.A., Jenks, W.S., 1999. Photocatalytic degradation of 4-chlorophenol. 1. The hydroquinone pathway. J. Org. Chem. 64 (23), 8509–8524.

Li, F., Wu, J.F., Qin, Q.H., Li, Z., Huang, X.T., 2010. Controllable synthesis, optical and photocatalytic properties of CuS nanomaterials with hierarchical structures. Powder Technol. 198 (2), 267–274.

Liu, X.H., Cui, W.B., Lv, X.K., Liu, W., Zhao, X.G., Li, D., et al., 2008. Exchange bias in antiferromagnetic coupled Fe3O4 + Cr2O3 nanocomposites. J. Phys. D. Appl. Phys. 41 (10), 105005.

Ma, Z.Y., Liu, H.Z., 2007. Synthesis and surface modification of magnetic particles for application in biotechnology and biomedicine. China Particuol. 5 (1-2), 1–10.

Massart, R., 1981. Preparation of aqueous magnetic liquids in alkaline and acidic media. IEEE Trans. Magn. 17 (2), 1247–1248.
Ramamoorthy, S., Ramamoorthy, S., 1997. Chlorinated Organic Compounds in the Environment: Regulatory and Monitoring Assessment. CRC Press, Florida, USA.
Santulli, A.C., Feygenson, M., Camino, F.E., Aronson, M.C., Wong, S.S., 2011. Synthesis and characterization of one-dimensional $Cr_2O_3$ nanostructures. Chem. Mater. 23 (4), 1000–1008.
Senapati, K.K., Borgohain, C., Sarma, K.C., Phukan, P., 2011. Photocatalytic degradation of methylene blue in water using $CoFe_2O_4$–$Cr_2O_3$–$SiO_2$ fluorescent magnetic nanocomposite. J. Mol. Catal. A Chem. 346 (1-2), 111–116.
Senapati, K.K., Borgohain, C., Phukan, P., 2012. $CoFe_2O_4$–ZnS nanocomposite: a magnetically recyclable photocatalyst. Catal. Sci. Technol. 2 (11), 2361–2366.
Tang, A.D., Xiao, Y., Ouyang, J., Nie, S., 2008. Preparation, photo-catalytic activity of cuprous oxide nano-crystallites with different sizes. J. Alloys Compd. 457 (1-2), 447–451.
Theurich, J., Lindner, M., Bahnemann, D.W., 1996. Photocatalytic degradation of 4-chlorophenol in aerated aqueous titanium dioxide suspensions: a kinetic and mechanistic study. Langmuir 12 (26), 6368–6376.
Tian, Y., Wu, D., Jia, X., Yu, B.B., Zhan, S.H., 2011. Core-shell nanostructure of $\alpha$-$Fe_2O_3$/$Fe_3O_4$: synthesis and photocatalysis for methyl orange. J. Nanomater. 2011, 1–5.
Tie, S.L., Lee, H.C., Bae, Y.S., Kim, M.B., Lee, K., Lee, C.H., 2007. Monodisperse $Fe_3O_4$/Fe@$SiO_2$ core/shell nanoparticles with enhanced magnetic property. Coll. Surf. A Physicochem. Eng. Asp. 293 (1-3), 278–285.
Tirosh, E., Shemer, G., Markovich, G., 2006. Optimizing cobalt ferrite nanocrystal synthesis using a magneto-optical probe. Chem. Mater. 18 (2), 465–470.
Wang, R., Xin, J.H., Yang, Y., Liu, H., Xu, L., Hu, J., 2004. The characteristics and photocatalytic activities of silver doped ZnO nanocrystallites. Appl. Surf. Sci. 227 (1-4), 312–317.
Yun, B.K., Koo, Y.S., Jung, J.H., 2009. Exchange bias in $Cr_2O_3$/$Fe_3O_4$ core/shell nanoparticles. J. Magn. 14 (4), 147–149.
Zhang, D.S., Du, Y.Q., 2006. The biocompatibility study of $Fe_3O_4$ magnetic nanoparticles used in tumor hyperthermia. Proceedings of the 1st IEEE International Conference on Nano/Micro Engineered and Molecular Systems. Zhuhai, China. Jan 18–21.
Zhu, Y., Stubbs, L.P., Ho, F., Liu, R., Ship, C.P., Maguire, J.A., et al., 2010. Magnetic nanocomposites: a new perspective in catalysis. ChemCatChem 2 (4), 365–374.
Znaidi, L., Pommier, C., 1998. Synthesis of nanometric chromium (III) oxide powders in supercritical alcohol. Eur. J. Solid State Inorg. Chem. 35 (6-7), 405–417.